Original Article
Entresto therapy effectively protects heart and lung against transverse aortic constriction induced cardiopulmonary syndrome injury in rat

Hung-I Lu[1], Meng-Shen Tong[2], Kuan-Hung Chen[3], Fan-Yen Lee[1,4,7], John Y Chiang[5], Sheng-Ying Chung[2], Pei-Hsun Sung[2,7*], Hon-Kan Yip[2,6,7,8,9*]

[1]Division of Thoracic and Cardiovascular Surgery, Department of Surgery, Kaohsiung Chang Gung Memorial Hospital and Chang Gung University College of Medicine, Kaohsiung 83301, Taiwan; [2]Division of Cardiology, Department of Internal Medicine, Kaohsiung Chang Gung Memorial Hospital and Chang Gung University College of Medicine, Kaohsiung 83301, Taiwan; [3]Department of Anesthesiology, Kaohsiung Chang Gung Memorial Hospital and Chang Gung University College of Medicine, Kaohsiung 83301, Taiwan; [4]Division of Cardiovascular Surgery, Department of Surgery, Tri-Service General Hospital, National Defense Medical Center, Taiwan; [5]Department of Computer Science and Engineering, National Sun Yat-sen University, Kaohsiung, Taiwan; [6]Institute for Translational Research in Biomedicine, [7]Center for Shockwave Medicine and Tissue Engineering, Kaohsiung Chang Gung Memorial Hospital, Kaohsiung 83301, Taiwan; [8]Department of Medical Research, China Medical University Hospital, China Medical University, Taichung 40402, Taiwan; [9]Department of Nursing, Asia University, Taichung 41354, Taiwan. *Equal contributors.

Abstract: This study tested the hypothesis that entresto therapy effectively protected heart and lung against cardiopulmonary syndrome (CPS) caused by transverse aortic constriction (TAC) in rat. Adult-Male SD rats (n = 36) were equally categorized into group 1 [sham-operated control (SC)], group 2 [SC + enalapril (7 mg/kg/day) since day-28 after TAC induction], group 3 [SC + entresto (30 mg/kg/day) since day-14 after TAC induction], group 4 (TAC only), group 5 (TAC + enalapril) and group 6 (TAC + entresto) and euthanized at day 60 after TAC induction. By day 60, the left-ventricular (LV) ejection fraction was significantly lower in group 4 than in other groups and significantly lower in groups 5 and 6 than in groups 1 to 3, whereas the ratios of heart and lung weights to tibial-length as well as the right-ventricular-systolic blood pressure exhibited an opposite pattern among the groups (all P<0.001). The sarcomere-length (SL), LV fibrotic area, cardiomyocyte size, and lung injury score were highest in group 4, lowest in groups 1 to 3 and significantly lower in group 6 than in group 5 (all P<0.0001). The protein expressions of fibrotic (Smad3/TGF-β), apoptotic (mitochondrial-Bax/cleaved-caspase3/PARP) and DNA-damaged (γ-H2AX) markers in lung and LV myocardium as well as oxidative (NOX-1/NOX2/oxidized protein) in LV myocardium exhibited an identical pattern of SL (all P<0.0001). The protein expressions of pressure/volume overload (BNP/MHC-β) mitochondrial-damaged (cytosolic cytochrome-C) of LV myocardium exhibited an identical pattern of SL (all P<0.001). In conclusion, Entresto is non-inferior to enalapril for protecting the heart-lung against CPS.

Keywords: Aortic constriction, cardiopulmonary syndrome, apoptosis, fibrosis, oxidative stress, entresto

Introduction

Hypertrophic cardiomyopathy (HCM) can be categorized into two casual etiologies, i.e., (1) due to a normal physiological stimulation, such as marathon running, weightlifting; and (2) due to pathological stimulation, for examples: HCM resulted from primary disease (i.e., genetic mutation), hypertension without treatment, aortic or supra-aortic valvular stenosis, or coarctation of aorta, etc. The HCM can elicit (1) heart failure (HF) in early stage without left ventricular (LV) chamber dilatation (i.e., HF in stage of LV preservation with diastolic dysfunction and poor compliance) and (2) late stage (i.e., end stage) of HF with LV dilatation and remodeling (i.e., decompensated HF in stage of LV dysfunction), that accounts for one of the most popular reasons of dilated cardiomyopathy (DCM). Accordingly, this kind of DCM is the end stage of HCM [1-4].

Copious etiologies can cause cardiopulmonary failure [i.e., called cardiopulmonary syndrome

(CPS)] [5-8]. The pathophysiological, hemodynamic and clinical studies have clearly established that HF caused by HCM/DCM associated with elevation of LV end-diastolic pressure that undoubtedly elicit elevations of left atrial and pulmonary capillary wedge pressures. Ultimately, the pulmonary, right ventricular, right atrial and systemic venous blood pressure elevations are clearly identified. This is the typical pathophysiology of both-side HF, named passive-caused "cardiopulmonary failure/syndrome". Despite state-of-the-art therapy, including advanced pharmacomodulation, cardiac intervention, circulatory mechanical device refinement, "keeping improving" cardiac rehabilitation program as well as constantly professionally guideline renew and recommendation, the long-term mortality rate in HF patients remains unchanged for the last 10 decades [5-13] regardless of the etiology. This raises the urgent need of finding a new and safe therapy for those of CPS patients.

Entresto is a novel drug for treatment of HF. Recently, some large randomized placebo-controlled clinical trials have shown that entresto therapy is superior to angiotensin converting enzyme inhibitor (ACEI) for improving the symptom/sign of HF, LV ejection fraction (LVEF) and clinical outcome in HF patients [14-17]. However, whether this drug therapy would reduce the HF caused by CPS and improve the prognostic outcome in setting of CPS has not yet been investigated. Accordingly, using an animal model, this study tested the therapeutic effect of entresto on protecting the heart and lung against CPS caused by transverse aortic constriction (TAC) in rat.

Materials and methods

Ethics

All animal experimental procedures were approved by the Institute of Animal Care and Use Committee at Kaohsiung Chang Gung Memorial Hospital (Affidavit of Approval of Animal Use Protocol No. 2016092906) and performed in accordance with the Guide for the Care and Use of Laboratory Animals [The Eighth Edition of the Guide for the Care and Use of Laboratory Animals (NRC 2011)].

Animals were housed in an Association for Assessment and Accreditation of Laboratory Animal Care International (AAALAC)-approved animal facility in our hospital with controlled temperature and light cycle (24°C and 12/12 light cycle).

Animal grouping and induction of pathological hypertrophic cardiomyopathy by transverse aortic constriction (TAC)

The pathogen-free, adult-male SD rats (n = 36) weighing 350-372 g (Charles River Technology, BioLASCO, Taiwan) were equally categorized into group 1 [sham-operated control (SC)], group 2 [SC + enalapril (Ena) (7 mg/kg/day) since day 14 after TAC induction], group 3 [SC + entresto (Ent) (30 mg/kg/day) since day 14 after TAC induction], group 4 (TAC only), group 5 (TAC + Ena) and group 6 (TAC + Ent).

The procedure and protocol of TCA have been described in our previous report [18]. In details, all animals were placed in a supine position under anesthesia with 2.0% inhalational isoflurane on a warming pad at 37°C and then intubated with positive-pressure ventilation (180 mL/min) with room air using a small animal ventilator (SAR-830/A, CWE, Inc., USA) for the TAC procedure. Under sterile conditions, the heart was exposed via a left thoracotomy procedure. TAC was induced in groups 4, 5 and 6 animals by tying firmly in the ascending aorta with a piece of 7-0 prolene on a 25# needle between the aortic arch [i.e., just beyond the right common carotid artery (CCA)] and left CCA. The needle was then removed, leaving a constricted aorta. These rats were then assigned to groups 4 to 6, respectively. Only a left thoracotomy without TAC was performed for groups 1 to 3 animals. After the TAC procedure, the thoracotomy wound was closed and the animals were allowed to recover from anaesthesia in a portable animal intensive care unit (ThermoCare®) for 24 hours.

The heart function of animals in each group was serially assessed during the study period. The study animals were euthanized at day 60 after TAC induction.

Rationale of the medications

The dosage of enalapril utilized in the present study were based on previous report [19] with minimal modification. Additionally, based on the component of valsartan in entresto is about 50% in weight (i.e., mg) and our previous study

[20] demonstrated that valsartan 10 mg/kg/day effectively protected the residual renal function in setting of chronic kidney disease in rat. Therefore, a minimal modification of entresto (i.e., 30 mg/kg/day) was utilized for each animal in the present study.

Assessment of heart function by echocardiography

The procedure and protocol of echocardiography have been descried in our previous report [18]. In details, transthoracic echocardiography was performed in each group prior to and on days 14, 30 and 60 after TAC induction. The procedure was performed by an expert animal technician blinded to the experimental design using an ultrasound machine (Vevo 2100, Visualsonics). M-mode standard two-dimensional (2D) left parasternal-long axis echocardiographic examination was conducted. Left ventricular internal dimensions [i.e., left ventricular end-systolic diameter (LVESd) and left ventricular end-diastolic diameter (LVEDd)] were measured at mitral valve level of left ventricle, according to the American Society of Echocardiography leading-edge method using at least three consecutive cardiac cycles. Left ventricular ejection fraction (LVEF) was calculated as follows: LVEF (%) = [(LVEDd^3-LVESd^3)/LVEDd^3] × 100%.

Hemodynamic studies and specimen preparation

The procedure and protocol were based on our previous report [21]. In details, on days 60 after TAC induction, the SD rats in all groups were anesthetized with inhalational 2.0% isoflurane. Each animal was endotracheally intubated with positive-pressure ventilation using 100% oxygen with a tidal volume of 250 μL at a rate of 120 breaths per minute using a Small Animal Ventilator (SAR-830/A, CWE, Inc., USA). The heart was exposed by left thoracotomy. A sterile 20-gauge, soft plastic needle was inserted into the right ventricle and femoral artery of each rat to measure the right ventricular systolic pressure (RVSP) and arterial systolic blood pressure (SBP), respectively. The pressure signals were first transmitted to pressure transducers (UFI, model 1050, CA, U.S.A.) and then exported to a bridge amplifier (ML866 PowerLab 4/30 Data Acquisition Systems; ADInstruments Pty Ltd., Castle Hill, NSW, Australia) where the

signals were amplified and digitized. The data were recorded and later analyzed with the Labchart software (ADInstrument). After hemodynamic measurements, the SD rats were euthanized with the left and right hearts and lungs harvested.

Western blot analysis

The procedure and protocol for Western blot analysis were based on our recent reports [18, 20-22]. Briefly, equal amounts (50 μg) of protein extracts were loaded and separated by SDS-PAGE using acrylamide gradients. After electrophoresis, the separated proteins were transferred electrophoretically to a polyvinylidene difluoride (PVDF) membrane (GE, UK). Nonspecific sites were blocked by incubating the membrane in blocking buffer [5% nonfat dry milk in T-TBS (TBS containing 0.05% Tween 20)] overnight. The membranes were incubated with the indicated primary antibodies [caspase 3 (1:1000, Cell Signaling), Poly (ADP-ribose) polymerase (PARP) (1:1000, Cell Signaling), mitochondrial Bax (1:1000, Abcam), γ-H2AX (1:1000, Cell Signaling), cytosolic cytochrome C (1:1000, BD), mitochondrial cytochrome C, phosphorylated (p)-Smad3 (1:1000, Cell Signaling), transforming growth factor (TGF)-β (1:500, Abcam), NOX-1 (1:1500, Sigma), NOX-2 (1:750, Sigma), brain natriuretic peptide (BNP) (1:500, Abcam), α-MHC (1:300, Santa Cruz), β-MHC (1:1000, Santa Cruz), COX-IV (1:1000, Abcam), and Actin (1:10000, Millipore)] for 1 hour at room temperature. Horseradish peroxidase-conjugated anti-rabbit immunoglobulin IgG (1:2000, Cell Signaling, Danvers, MA, USA) was used as a secondary antibody for one-hour incubation at room temperature. The washing procedure was repeated eight times within one hour. Immunoreactive bands were visualized by enhanced chemiluminescence (ECL; Amersham Biosciences, Amersham, UK) and exposed to Biomax L film (Kodak, Rochester, NY, USA). For the purpose of quantification, ECL signals were digitized using Labwork software (UVP, Waltham, MA, USA).

Immunohistochemical (IHC) and immunofluorescent (IF) staining

The procedure and protocol of IHC and IF staining have been described in detail in our previous reports [18, 20-22]. For IHC and IF staining, rehydrated paraffin sections were first treated

with 3% H_2O_2 for 30 minutes and incubated with Immuno-Block reagent (BioSB, Santa Barbara, CA, USA) for 30 minutes at room temperature. Sections were then incubated with primary antibodies specifically against Sirius red, Masson's trchrome (ScyTek Lab), transient receptor potential cation channel 1 (TRPC1) (1:200, Abcam), TRPC4 (1:200, GeneTex) and sarcomere (1:500, Imgenx), while sections incubated with the use of irrelevant antibodies served as controls. Three sections of heart and lung specimens from each rat were analyzed. For quantification, three randomly selected HPFs (200× for IF studies) were analyzed in each section. The staining and identification of TRPC1 and TRPC4 were based on our previous reports [23, 24].

Assessment of oxidative stress

The procedure and protocol for evaluating the protein expression of oxidative stress have been described in detail in our previous reports [25-27]. The Oxyblot Oxidized Protein Detection Kit was purchased from Chemicon, Billerica, MA, USA (S7150). DNPH derivatization was carried out on 6 μg of protein for 15 minutes according to the manufacturer's instructions. One-dimensional electrophoresis was carried out on 12% SDS/polyacrylamide gel after DN-PH derivatization. Proteins were transferred to nitrocellulose membranes that were then incubated in the primary antibody solution (anti-DNP 1:150) for 2 hours, followed by incubation in secondary antibody solution (1:300) for 1 hour at room temperature. The washing procedure was repeated eight times within 40 minutes. Immunoreactive bands were visualized by enhanced chemiluminescence (ECL; Amersham Biosciences, Amersham, UK) which was then exposed to Biomax L film (Kodak, Rochester, NY, USA). For quantification, ECL signals were digitized using Labwork software (UVP, Waltham, MA, USA). For oxyblot protein analysis, a standard control was loaded on each gel.

Estimation of cardiomyocyte size and arterial masculinization in lung parenchyma

Microscopic finding of H&E stain was utilized as determinant of the cardiomyocyte size in each animal under the HPFs (i.e., 400×) in cross-section of heart specimen. Three sections of heart specimen from each rat were analyzed. For quantification, three randomly selected HPFs (non-overlapping fields) were analyzed in each section. Finally, the summation of area of total cells was divided by the number of cells and three randomly selected views of them were calculated.

Histological assessment of lung injury score and crowded score of lung parenchyma by day 60 after TCA induction

For identification of number of alveolar sac distribution in lung parenchyma, left lung specimens from all animals were fixed in 4% parafomaldehyde prior to embedding in paraffin and the lung tissue was sectioned at 5 μm for light microscopic analysis. The H&E stain was performed for assessment of number of alveolar sacs based on our previous reports [23, 26] in a blind fashion. Three lung sections from each rat were analyzed with three randomly selected HPFs (i.e., 100×) in each section. The mean number per HPF for each animal was then determined by summation of all numbers divided by 9. The extent of crowded area, defined as region of thickened septa in lung parenchyma associated with partial or complete collapse of alveoli on H&E-stained sections, was performed in a blind fashion. The scoring system adopted was as follows: 0 = no detectable crowded area; 1 ≤ 15% of crowded area; 2 = 15-25% of crowded area; 3 = 25-50% of crowded area; 4 = 50-75% of crowded area; 5 ≥ 75%-100% of crowded area/per high-power filed (100×).

Histological quantification of myocardial fibrosis and collagen deposition in LV myocardium

The procedure and protocol have been described in our previous studies [25, 28]. In details, Masson's trichrome staining was used for identifying the fibrosis of LV myocardium. Three serial sections of LV myocardium in each animal at the same levels were prepared at 4 μm thickness by Cryostat (Leica CM3050S). The integrated area ($μm^2$) of infarct area and fibrosis on each section were calculated using the Image Tool 3 (IT3) image analysis software (University of Texas, Health Science Center, San Antonio, UTHSCSA; Image Tool for Windows, Version 3.0, USA). Three randomly selected HPFs (100×) were analyzed in each section. After assessment of the number of pixels in each fibrotic area per HPF, the numbers of pixels obtained from three HPFs were summed. The procedure was repeated in two other sections for each animal. The mean pixel
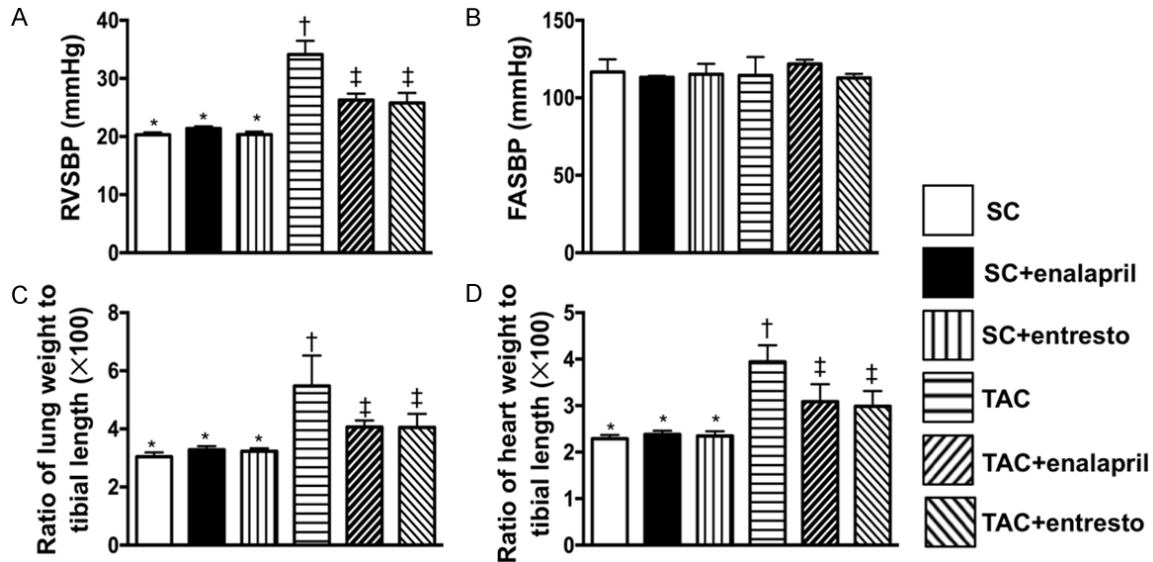
Figure 1. The hemodynamic parameters and anatomically pathological features of heart and lung by day 60 after TAC induction. A. Right ventricular systolic blood pressure, * vs. other groups with different symbols (†, ‡), P<0.0001. B. Right femoral arterial systolic blood pressure (FASBP), P>0.5. C. Ratio of total lung weight to tibial length, * vs. other groups with different symbols (†, ‡), P<0.0001. D. The ratio of total heart weight to tibial length, *vs. other groups with different symbols (†, ‡), P<0.0001. All statistical analyses were performed by one-way ANOVA, followed by Bonferroni multiple comparison post hoc test (n = 6 for each group). Symbols (*, †, ‡) indicate significance at the 0.05 level. SC = sham-operated control; TAC = transverse aortic constriction.

number per HPF for each animal was then calculated by summing up all pixel numbers and dividing by 9. The mean integrated area (µm²) of fibrosis in LV myocardium per HPF was obtained using a conversion factor of 19.24 (1 µm² represented 19.24 pixels).

To analyze the extent of collagen synthesis and deposition, cardiac paraffin sections (6 µm) were stained with picrosirius red (1% Sirius red in saturated picric acid solution) for one hour at room temperature using standard methods. The sections were then washed twice with 0.5% acetic acid. The water was physically removed from the slides by vigorous shaking. After dehydration in 100% ethanol thrice, the sections were cleaned with xylene and mounted in a resinous medium. HPFs (×400) of each section were utilized to identify Sirius red-positive area on each section. Analyses of condensed collagen deposition area in LV myocardium were performed exactly according to the aforementioned description for the calculations of the fibrotic area.

Statistical analysis

Quantitative data are expressed as means ± SD. Statistical analysis was adequately performed by ANOVA, followed by Bonferroni multi-

ple-comparison post hoc test. SAS statistical software for Windows version 8.2 (SAS institute, Cary, NC) was utilized. A *P* value of less than 0.05 was considered statistically significant.

Results

*The hemodynamic parameters and anatomically pathological features of heart and lung by day 60 after TAC induction (**Figure 1**)*

By day 60 after TAC induction, the RVSBP, an indirect reflection of pulmonary artery systolic blood pressure (PASBP), was significantly increased in TAC than in the other groups and significantly increased in TAC-Ena and TAC-Ent than in SC, SC-Ena and SC-Ent, but it did not differ between TAC-Ena and TAC-Ent or among the SC, SC-Ena and SC-Ent. On the other hand, the femoral arterial SBP was similar among the 6 groups. Additionally, the ratios of total lung weight and total heart weight to tibial length were identical to the RVSBP among the six groups.

*Time courses of LVEF and cardiomyocyte size of LV myocardium by day 60 after TAC (**Figure 2**)*

The baseline LVEF was similar among the six groups. However, by day 14 after the TCA induc-
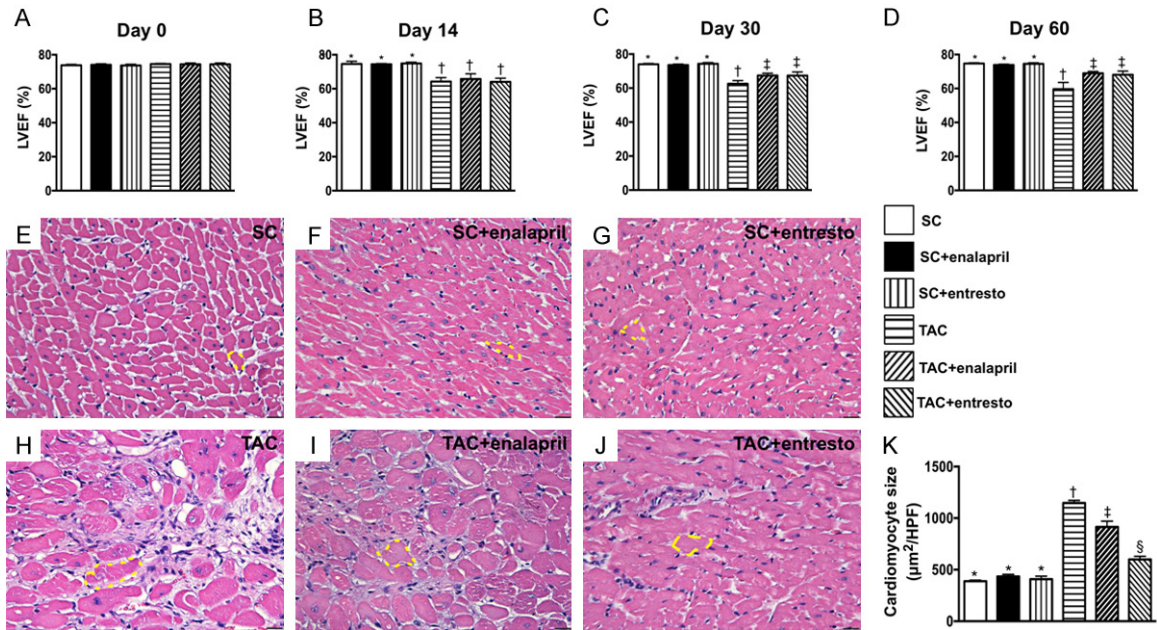
Figure 2. Time courses of LVEF and cardiomyocyte size of LV myocardium by day 60 after TAC. A. Analytical result of LVEF at day 0, P>0.5. B. Analytical result of LVEF at day 14 after TAC procedure, * vs. †, P<0.001. C. Analytical result of LVEF at day 30 after TAC procedure, * vs. other groups with different symbols (†, ‡), P<0.001. D. Analytical result of LVEF at day 60 after TAC procedure, *vs. other groups with different symbols (†, ‡), P<0.001. E-J. Illustrating the microscopic finding (400×) of H&E stain for identification of cardiomyocyte size. Yellow dotted line indicated one cardiomyocyte. K. Analytical result of cardiomyocyte size at day 60 after TAC procedure, *vs. other groups with different symbols (†, ‡), P<0.0001. Scale bars in right lower corner represent 20 μm. All statistical analyses were performed by one-way ANOVA, followed by Bonferroni multiple comparison post hoc test (n = 6 for each group). Symbols (*, †, ‡) indicate significance at the 0.05 level. SC = sham-operated control; TAC = transverse aortic constriction; LVEF = left ventricular ejection fraction.

tion, the LVEF was significantly lower in TAC, TAC-Ena and TAC-Ent than in SC, SC-Ena and SC-Ent, but it showed no difference among the former three groups or the latter three groups. By days 30 and 60, after TAC induction, the LVEF remained significantly higher in SC, SC-Ena and SC-Ent than in TAC, TAC-Ena and TAC-Ent. However, this parameter was significantly higher in TAC-Ena and TAC-Ent than in TAC, but no difference between TAC-Ena and TAC-Ent or among SC, SC-Ena and SC-Ent. On the other hand, by day 60 after TAC procedure, the cardiomyocyte size was highest in TAC and lowest in SC, SC-Ena and SC-Ent, and significantly higher in TAC-Ena than in TAC-Ent.

Identification of fibrotic and collagen-deposition area in LV myocardium and lung injury score by day 60 after TAC induction (Figures 3 and 4)

The fibrotic and collagen deposition areas were significantly higher in TAC than in other groups, significantly higher in TAC-Ena and TAC-Ent than

in SC, SC-Ena and SC-Ent and significantly higher in TAC-Ena than in TAC-Ent, but no difference among the three control groups.

Additionally, the lung crowded score, an indicator of lung injury score, displayed an identical pattern to the fibrotic area among the six groups. On the other hand, the number of alveolar sacs, an indicator of integrity of lung parenchyma, showed an opposite pattern to the fibrotic area among the six groups.

Sarcomere length and protein expression of pressure-volume overload and mitochondrial-damaged markers by day 60 after TAC induction (Figure 5)

IF microscopic finding showed that the sarcomere length was significantly increased in TAC than in other groups, significantly increased in TAC-Ena and TAC-Ent than in SC, SC-Ena and SC-Ent and significantly increased in TAC-Ena than in TAC-Ent, but similar among the SC, SC-Ena and SC-Ent.
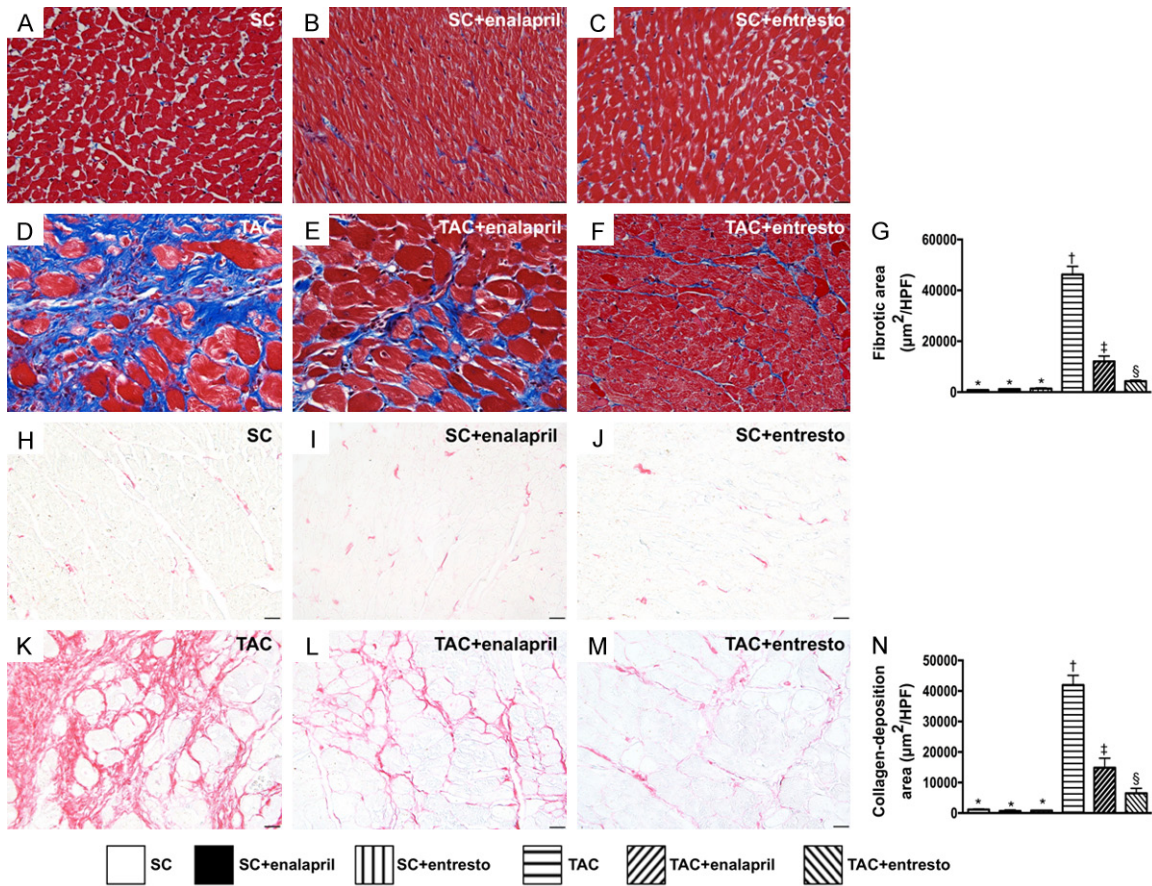
Figure 3. Identifications of fibrotic and condensed collagen-deposition areas in LV myocardium and lung injury score by day 60 after TAC induction. A-F. Illustrating the microscopic finding (400×) of Masson's trichome stain for identification of fibrosis (blue color). G. Analytical results of fibrotic area, * vs. other groups with different symbols (†, ‡, §), P<0.0001. H-M. Showing the microscopic finding (400×) of Sirius red stain for identification of condensed collagen-deposition area (pink color). N. Analytical result of collagen-deposition area, * vs. other groups with different symbols (†, ‡, §), P<0.0001. The scale bars in right lower corner represent 20 μm. All statistical analyses were performed by one-way ANOVA, followed by Bonferroni multiple comparison post hoc test (n = 6 for each group). Symbols (*, †, ‡) indicate significance at the 0.05 level. SC = sham-operated control; TAC = transverse aortic constriction; LV = left ventricular.
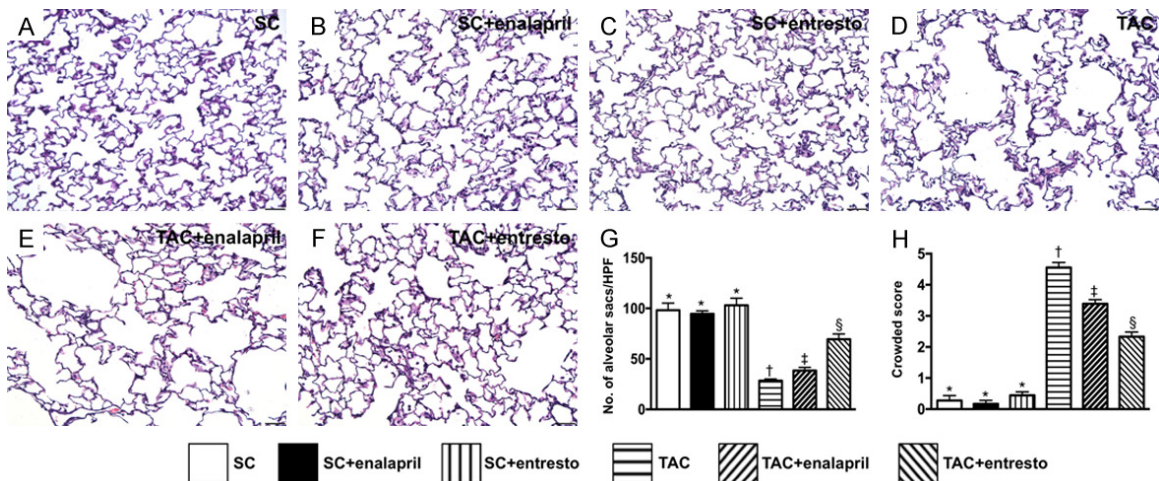
Figure 4. Histopathological findings in lung parenchyma by day 60 after TAC induction. A-F. Histopathological findings (i.e., H&E staining) of lung parenchyma under microscopy (200×) among the five groups. G. Analytic results of

number of alveolar sacs, *vs. other groups with different symbols (†, ‡, §), P<0.0001. H. Analytic results of crowded score, *vs. other groups with different symbols (†, ‡, §), P<0.0001. The scale bars in right lower corner represent 50 μm. All statistical analyses were performed by one-way ANOVA, followed by Bonferroni multiple comparison post hoc test (n = 6 for each group). Symbols (*, †, ‡) indicate significance at the 0.05 level. SC = sham-operated control; TAC = transverse aortic constriction; HPF = high-power field.
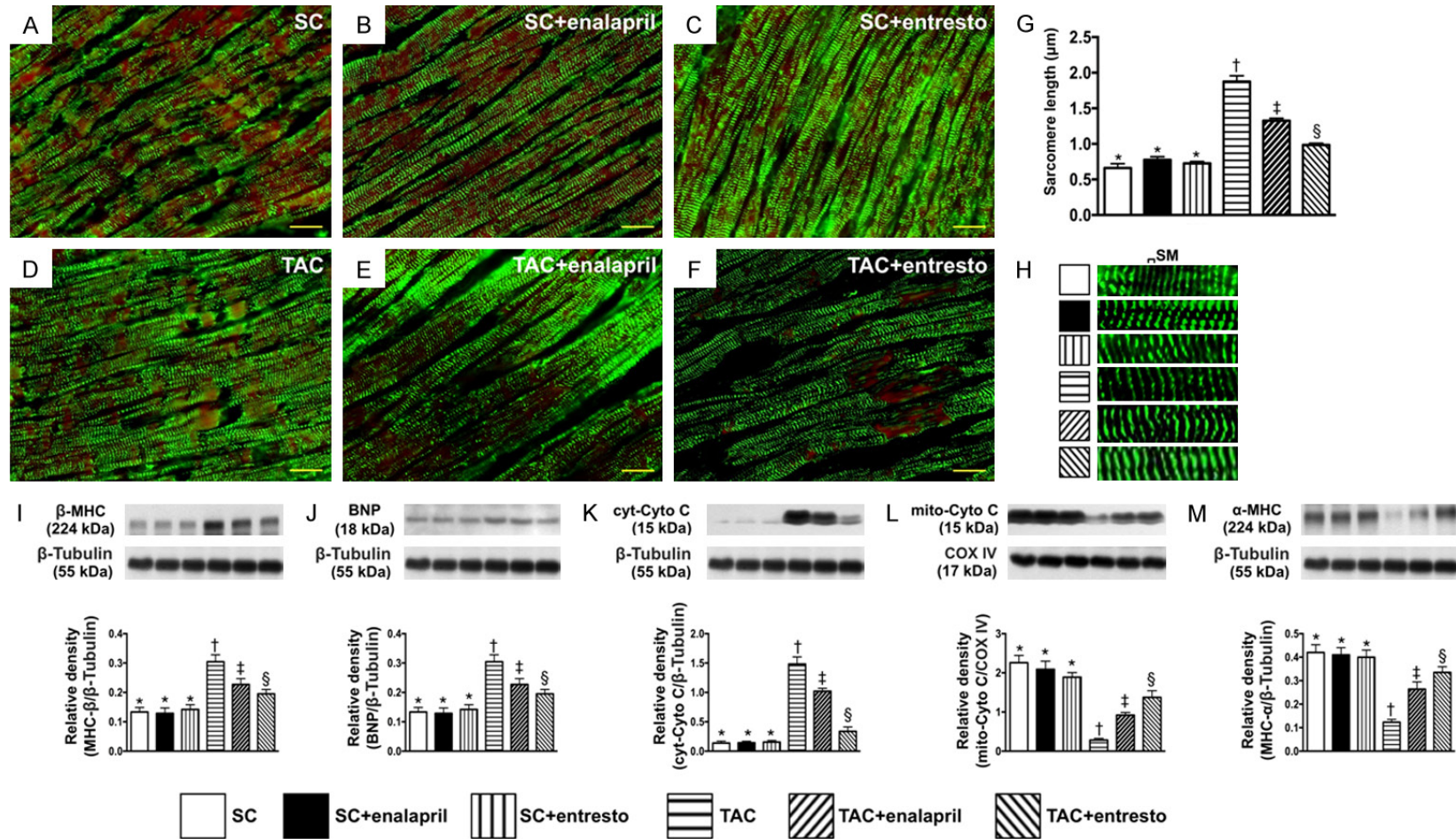
Figure 5. Actinin-phalloidin staining for measuring the sarcomere length of cardiomyocytes and protein expression of pressure-volume overload and mitochondrial-damaged markers in LV myocardium by day 60 after TAC induction. A-F. Showing the microscopic finding (630×) of immunofluorescent stain for identifying LV sarcomere length (green striatum). G. Results of statistical analysis, * vs. other groups with different symbols (†, ‡, §), P<0.0001. The scale bars in right lower corner represent 10 μm. H. Illustrating the measurement (magnified **Figure 5A-F**) of distance of sarcomere length. SM = sarcomere length. I. Protein expression of β-myosin heavy chain (MHC) protein expression, *vs. other groups with different symbols (†, ‡, §), P<0.0001. J. Protein expressions of brain natriuretic peptide (BNP), *vs.

other groups with different symbols (†, ‡), P<0.0001. K. Protein expression of cytosolic cytochrome C (cyt-Cyto C), *vs. other groups with different symbols (†, ‡, §), P<0.0001. L. Protein expression of mitochondrial cytochrome C (mit-Cto C), *vs. other groups with different symbols (†, ‡, §), P<0.0001. M. Protein expression of MHC-α, *vs. other groups with different symbols (†, ‡, §), P<0.0001. All statistical analyses were performed by one-way ANOVA, followed by Bonferroni multiple comparison post hoc test (n = 6 for each group). Symbols (*, †, ‡) indicate significance at the 0.05 level. SC = sham-operated control; TAC = transverse aortic constriction; LV = left ventricular.
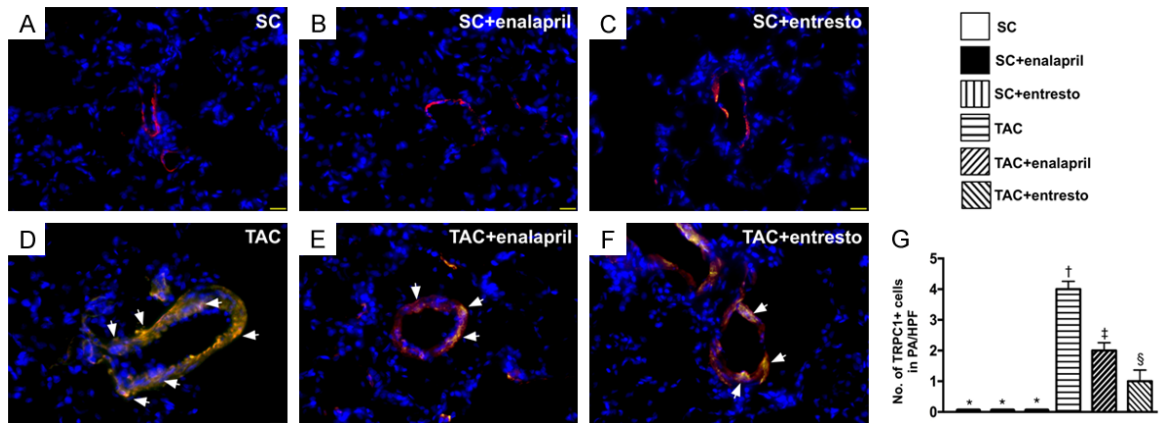
Figure 6. Immunofluorescent (IF) staining for the expression of TRPC1 in pulmonary artery (PA) by day 60 after TAC induction. A-F. Illustrating the microscopic finding for identification of **transient receptor potential cation channel 1** (TRPC1)+ cells in PA (white arrow) using IF double staining (i.e., α-SMA-TRPC1) in the six groups (400×). G. Analytical result of number of positively-stained TRPC1+ cells in PA, *vs. other groups with different symbols (†, ‡, §), P<0.001. The scale bars in right lower corner represent 20 μm. All statistical analyses were performed by one-way ANOVA, followed by Bonferroni multiple comparison post hoc test (n = 6 for each group). Symbols (*, †, ‡) indicate significance at the 0.05 level. SC = sham-operated control; TAC = transverse aortic constriction; HPF = high-power field.
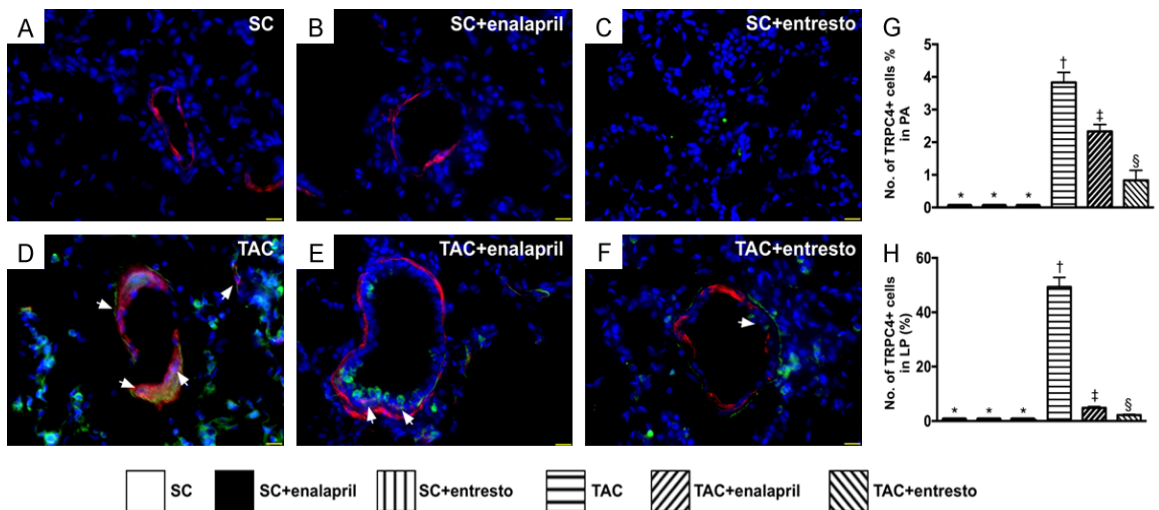
Figure 7. Immunofluorescent (IF) staining for the expression of TRPC2 in pulmonary artery (PA) and lung parenchyma (LP) by day 60 after TAC induction. A-F. Illustrating the microscopic finding for identification of **transient receptor potential cation channel 1** (TRPC4)+ cells in PA (white arrow) using IF double staining (i.e., α-SMA-TRPC1) in the six groups (400×). G. Analytical result of number of positively-stained TRPC4+ cells in PA, *vs. other groups with different symbols (†, ‡, §), P<0.001. The scale bars in right lower corner represent 20 μm. H. Analytical result of number of TRPC4+ cells in PL, *vs. other groups with different symbols (†, ‡, §), P<0.0001. All statistical analyses were performed by one-way ANOVA, followed by Bonferroni multiple comparison post hoc test (n = 6 for each group). Symbols (*, †, ‡) indicate significance at the 0.05 level. SC = sham-operated control; TAC = transverse aortic constriction.
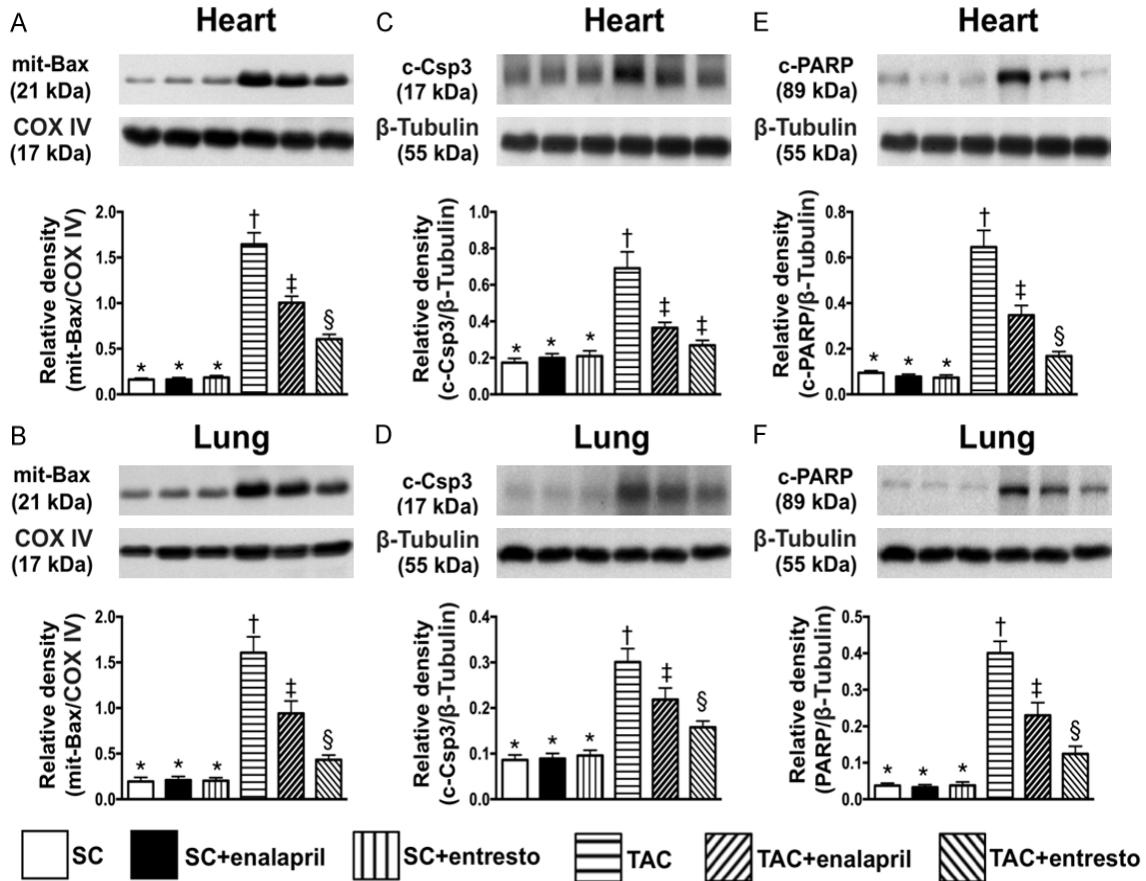
Figure 8. The protein expression of apoptosis in lung and heart by day 60 after TAC induction. A. Protein expression of mitochondrial (mit)-Bax in LV myocardium, *vs. other groups with different symbols (†, ‡, §), P<0.0001. B. Protein expression of mit-Bax in lung, *vs. other groups with different symbols (†, ‡, §), P<0.0001. C. Protein expression of cleaved caspase 3 (c-Csp 3) in LV myocardium, *vs. other groups with different symbols (†, ‡), P<0.0001. D. Protein expression of c-Csp 3 in LV myocardium, * vs. other groups with different symbols (†, ‡, §), P<0.0001. E. Protein expression of cleaved poly (ADP-ribose) polymerase (c-PARP) in LV myocardium, *vs. other groups with different symbols (†, ‡), P<0.001. F. Protein expression of c-PARP in lung, * vs. other groups with different symbols (†, ‡), P<0.001. All statistical analyses were performed by one-way ANOVA, followed by Bonferroni multiple comparison post hoc test (n = 6 for each group). Symbols (*, †, ‡) indicate significance at the 0.05 level. SC = sham-operated control; TAC = transverse aortic constriction; LV = left ventricular.

It is well recognized that cardiac hypertrophy is characterized by a switch from α- to β-MHC protein expression (i.e. reactivation of fetal gene program). The protein expressions of BNP and β-MHC, two indicators of pressure-volume over-load biomarkers, and cytosolic cytochrome C, an indicator of mitochondrial-damaged markers, exhibited an identical pattern to the sarcomere length among the six groups. On the other hand, the protein expression of mitochondrial cytochrome C, an indicator of mitochondrial integrity, and protein expression of MHC-α, an opposite indicator of cardiac hypertrophy, revealed an opposite pattern of BNP among the six groups.

*The expressions of TRPC1 and TRPC4 in pulmonary artery by day 60 after TAC induction (**Figures 6** and 7)*

TRPCs play particularly crucial roles in regulating smooth muscle cell contraction and proliferation in the murine model of hypoxia-induced pulmonary arterial hypertension [24, 27]. IF microscopic findings showed that the cellular expressions of TRPC1 (**Figure 6**) and TRPC4 (**Figure 7**) in pulmonary artery were significantly higher in TAC than in other groups, significantly higher in TAC-Ena and TAC-Ent than in SC, SC-Ena and SC-Ent and significantly higher in TAC-Ena than in TAC-Ent, yet no difference
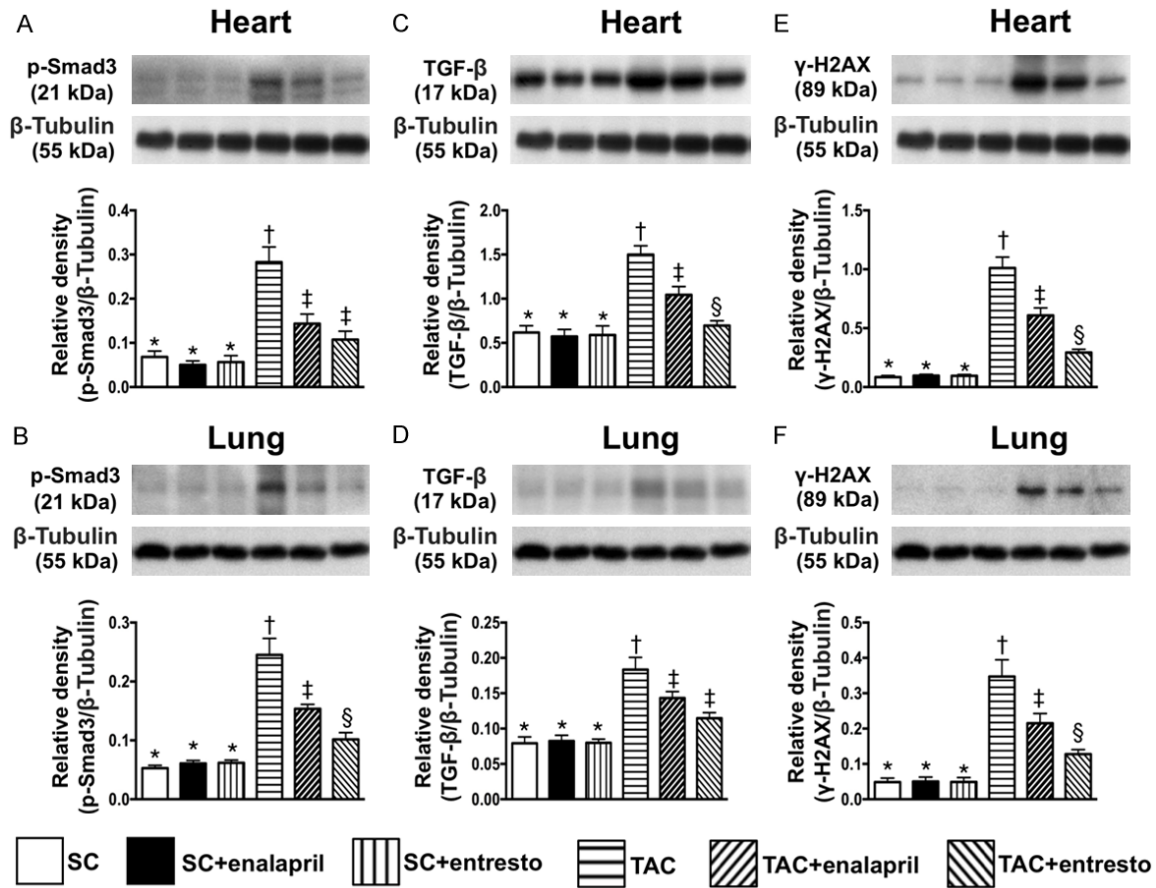
Figure 9. The protein expressions of fibrotic and DNA-damaged biomarkers in lung and heart by day 60 after TAC induction. A. Protein expression of Smad3 in LV myocardium, * vs. other groups with different symbols (†, ‡), P<0.0001. B. Protein expression of Smad3 in lung, * vs. other groups with different symbols (†, ‡, §), P<0.0001. C. Protein expression of transforming growth factor (TGF)-β in LV myocardium, *vs. other groups with different symbols (†, ‡, §), P<0.0001. D. Protein expression of TGF-β in lung, *vs. other groups with different symbols (†, ‡), P<0.0001. E. Protein expression of γ-H2AX in LV myocardium, *vs. other groups with different symbols (†, ‡, §), P<0.0001. F. Protein expression of γ-H2AX in lung, * vs. other groups with different symbols (†, ‡, §), P<0.0001. All statistical analyses were performed by one-way ANOVA, followed by Bonferroni multiple comparison post hoc test (n = 6 for each group). Symbols (*, †, ‡) indicate significance at the 0.05 level. SC = sham-operated control; TAC = transverse aortic constriction; LV = left ventricular.

among the SC, SC-Ena and SC-Ent. Additionally, the number of positively-stained TRPC4 in lung parenchyma exhibited an identical pattern of TRPC4 in PA among the groups.

The protein expression of apoptosis in lung and heart by day 60 after TAC induction (Figure 8)

The protein expressions of mitochondrial Bax, cleaved caspase3 and cleaved PARP in lung and LV myocardium, three indices of apoptosis, were significantly higher in TAC than in other groups, significantly higher in TAC-Ena and TAC-Ent than in SC, SC-Ena and SC-Ent, and signifi-

cantly higher in TAC-Ena than in TAC-Ent, but no difference was observed among the SC, SC-Ena and SC-Ent.

The protein expressions of fibrotic and DNA-damaged biomarkers in lung and heart by day 60 after TAC induction (Figure 9)

The protein expressions of Smad3 and TGF-β, two indicators of fibrosis, and the protein expression of γ-H2AX, an indicator of DNA-damaged markers in lung and LV myocardium, were significantly higher in TAC than in other groups, significantly higher in TAC-Ena and TAC-Ent than in SC, SC-Ena and SC-Ent, and signifi-
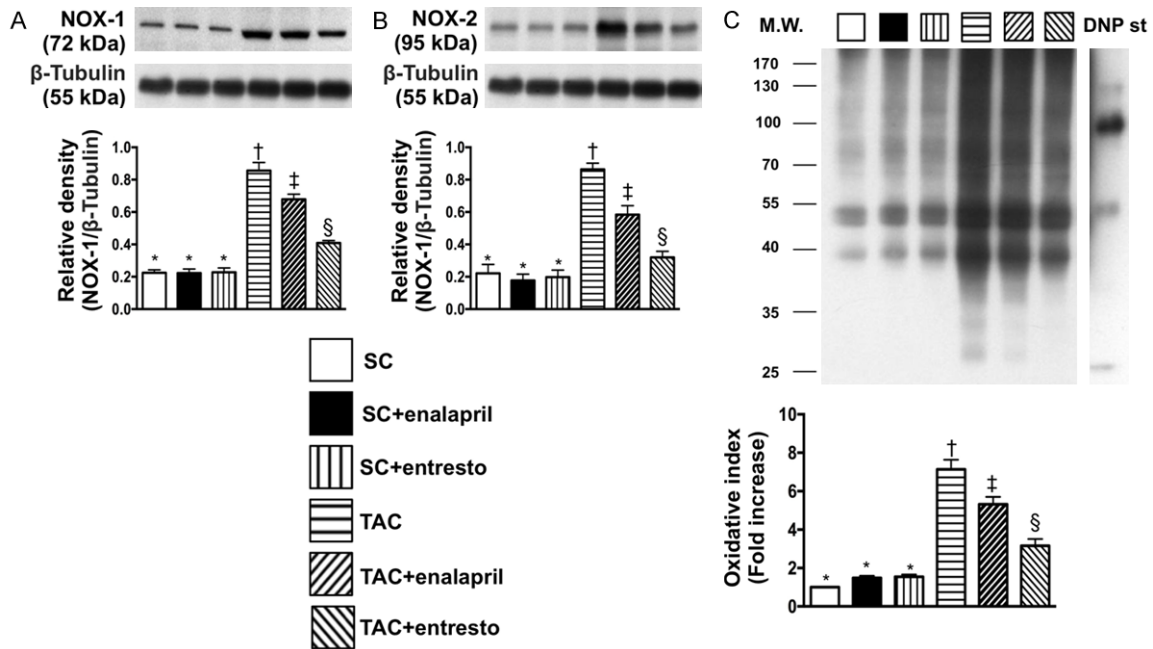
Figure 10. The protein expressions of oxidative stress in LV myocardium by day 60 after TAC induction. A. Protein expressions of NOX-1, *vs. other groups with different symbols (†, ‡, §), P<0.0001. B. Protein expressions of NOX-2, *vs. other groups with different symbols (†, ‡, §), P<0.0001. C. Oxidized protein expression, *vs. other groups with different symbols (†, ‡), P<0.0001. (Note: left and right lanes shown on the upper panel represent protein molecular weight marker and control oxidized molecular protein standard, respectively). M.W = molecular weight; DNP = 1-3 dinitrophenylhydrazone. All statistical analyses were performed by one-way ANOVA, followed by Bonferroni multiple comparison post hoc test (n = 6 for each group). Symbols (*, †, ‡) indicate significance at the 0.05 level. SC = sham-operated control; TAC = transverse aortic constriction; LV = left ventricular.

cantly higher in TAC-Ena than in TAC-Ent, but maintained the same level among the SC, SC-Ena and SC-Ent.

The protein expressions of oxidative stress in LV myocardium by day 60 after TAC induction (Figure 10)

The protein expressions of NOX-1 and NOX-2 and oxidized protein, three indices of oxidative stress in LV myocardium, were significantly higher in TAC than in other groups, significantly higher in TAC-Ena and TAC-Ent than in SC, SC-Ena and SC-Ent, and significantly higher in TAC-Ena than in TAC-Ent, but no difference among the SC, SC-Ena and SC-Ent.

Discussion

This study which investigated the therapeutic impact of entresto on protecting the heart and lung against CPS injury in rat yielded several striking implications. Frist, the results of the present study identified that, as compared to the controls, the ratios of heart and lung weight to tibial length and the sarcomere length of LV

myocardium were substantially increased in TAC animals, suggesting that we had successfully created a platform for preclinical study of therapeutic impact of entresto on CPS in rodent animals. Second, the results of the present study demonstrated that therapeutic effect of entresto was not inferior to enalapril on preserving the heart function and attenuating the lung and heart injury in setting of CPS. Third, as compared with control animals, the molecular-cellular perturbations were remarkably increased in CPS animals that were significantly reversed in those of CPS animals after receiving entresto or enalapril treatment.

One important finding in the present study was that the ratio of heart weight to tibial length, the cardiomyocyte size and the sarcomere length (i.e., anatomical indices) were significantly higher in CPS animals than in those of SC animals, suggesting that TAC procedure already induced LV remodeling. On the other hand, the LVEF (i.e., functional index) was notably reduced in CPS animals than in that of SC animals at the time intervals of days 14, 30 and 60 after TAC

procedure. However, these parameters were markedly reversed in CPS animals after receiving enalapril or entresto treatment. The cardioprotective effect of angiotensin II type I inhibitors (ARBs) on ischemic heart disease in rodent has been well recognized by our previous studies [20, 29, 30]. Accordingly, our findings are compatible with those of our previous studies [20, 29, 30]. Another important finding was that the ratio of lung weight to tibial length (i.e., anatomical indicator) and RVSBP, an indicator of PASBP (i.e., hemodynamic index), were significantly increased in CPS group than in SC groups. Contrary to the anatomical and hemodynamic parameters, the number of alveolar sacs was significantly decreased in CPS group than in control groups. As expected, these parameters were improved in CPS animals after receiving either enalapril or entresto treatment. Our findings highlight that entresto is not inferior to enalapril for protecting the lung and heart against TAC-induced CPS injury.

The fibrosis and collagen deposition have been identified as the final pathological findings in ischemic heart disease, including in the setting of DCM/HCM [18, 20, 22, 25, 28, 31]. Additionally, the crowded phenomenon of septum and alveoli (i.e., refer to as lung injury score) [21, 23, 24, 26] has been established to frequently occur in various setting of lung parenchymal diseases. An essential finding in the present study was that the fibrotic and condensed-collagen deposition areas in LV myocardium were significantly higher in CPS animals than in SC animals. Additionally, the lung injury score was notably increased in CPS animals than in SC animals. Our findings, in addition to strengthening the findings of previous studies [18, 20-22, 24, 26, 28, 31], could partially explain why the LV performance (i.e., LVEF) was significantly impaired and the RVSBP was notably increased in those of CPS animals. Of importance was these parameters were significantly reversed in CPS animals after receiving enalapril treatment and further significantly reversed by the entresto treatment.

BNP and MHC-β are two crucial biomarkers for prediction of pressure-volume overload in experimental studies [25, 28]. A principal finding in the present study was that these two parameters were significantly increased in LV myocardium of CPS animals than in the SC animals. Importantly, these two parameters were significantly reduced in CPS animals after receiving enalapril treatment and furthermore significantly reduced after the entresto treatment. Our findings, in addition to be consistent with those of previous studies [25, 28], could, at least in part, explain why the cardiac remodeling and the RVSBP were significantly reduced in CPS animals after administration of these two medicines.

Recently, abundant data from clinical trials [17, 32] have shown that entresto is superior to enalapril in reducing the risks of death and of hospitalization for HF as well as prevents the clinical progression of surviving patients with HF. However, the underlying mechanism for the improvement of clinical outcomes through entresto treatment is currently unclear. Another principal finding in the present study was that as compared to the SC animals, the protein levels of fibrosis and apoptosis in lung parenchyma and LV myocardium were remarkably higher in the CPS animals. Additionally, the protein levels of oxidative stress biomarkers in LV myocardium were also significantly higher in CPS animals than in SC animals. However, all of these molecular perturbations were significantly suppressed by enalapril therapy and further significantly suppressed by entresto therapy. These findings may be considered, at least in part, as the underlying mechanism for explaining the results from those of clinical trials [17, 32] and again shed light on why the LV function was preserved in CPS animals after receiving the entresto treatment.

Study limitation

This study has limitations. First, this study did not titrate the dosages of enalapril and entresto. Thus, the optimal dosage of these two drugs for the animals remains to be determined. Accordingly, whether the therapeutic effect of entresto on CPS is superior to enalapril or vice versa is currently uncertain. Second, the exactly underlying mechanism of enalapril and entresto for improving outcomes in CPS animals has not fully investigated in the current study.

In conclusion, entresto is comparable with enalapril for protecting the heart-lung organs against CPS-induced injury.

Disclosure of conflict of interest

None.

Address correspondence to: Drs. Hon-Kan Yip and Pei-Hsun Sung, Division of Cardiology, Department of Internal Medicine, Kaohsiung Chang Gung Memorial Hospital and Chang Gung University College of Medicine, Kaohsiung 83301, Taiwan. Tel: +886-7-7317123; Fax: +886-7-7322402; E-mail: han.gung@msa.hinet.net (HKY); Tel: +886-7-7317123; Fax: +886-7-7322402; E-mail: e12281@cgmh.org.tw (PHS)

References

[1] Guo J, Mihic A, Wu J, Zhang Y, Singh K, Dhingra S, Weisel RD and Li RK. Canopy 2 attenuates the transition from compensatory hypertrophy to dilated heart failure in hypertrophic cardiomyopathy. Eur Heart J 2015; 36: 2530-2540.

[2] Machii M, Satoh H, Shiraki K, Saotome M, Urushida T, Katoh H, Takehara Y, Sakahara H, Ohtani H, Wakabayashi Y, Ukigai H, Tawarahara K and Hayashi H. Distribution of late gadolinium enhancement in end-stage hypertrophic cardiomyopathy and dilated cardiomyopathy: differential diagnosis and prediction of cardiac outcome. Magn Reson Imaging 2014; 32: 118-124.

[3] Xiao Y, Yang KQ, Yang YK, Liu YX, Tian T, Song L, Jiang XJ and Zhou XL. Clinical characteristics and prognosis of end-stage hypertrophic cardiomyopathy. Chin Med J (Engl) 2015; 128: 1483-1489.

[4] Ziolkowska L, Turska-Kmiec A, Petryka J and Kawalec W. Predictors of long-term outcome in children with hypertrophic cardiomyopathy. Pediatr Cardiol 2016; 37: 448-458.

[5] Baek JK, Lee JS, Kim TH, Kim YH, Han DJ and Hong SK. Four-year experience with extracorporeal membrane oxygenation for kidney transplant patients with severe refractory cardiopulmonary insufficiency. Transplant Proc 2016; 48: 2080-2083.

[6] Dharmarajan K, Strait KM, Tinetti ME, Lagu T, Lindenauer PK, Lynn J, Krukas MR, Ernst FR, Li SX and Krumholz HM. Treatment for multiple acute cardiopulmonary conditions in older adults hospitalized with pneumonia, chronic obstructive pulmonary disease, or heart failure. J Am Geriatr Soc 2016; 64: 1574-1582.

[7] Huang M, Du W, Liu J, Zhang H, Cao L, Yang W, Zhang H, Wang Z, Wei P, Wu W, Huang Z, Fang Y, Lin Q, Qin X, Zhang Z, Zhou K and Zeng J. Interleukin-27 as a novel biomarker for early cardiopulmonary failure in enterovirus 71-infected children with central nervous system involvement. Mediators Inflamm 2016; 2016: 4025167.

[8] Mori-Yoshimura M, Segawa K, Minami N, Oya Y, Komaki H, Nonaka I, Nishino I and Murata M. Cardiopulmonary dysfunction in patients with limb-girdle muscular dystrophy 2A. Muscle Nerve 2017; 55: 465-469.

[9] Bonsu KO, Owusu IK, Buabeng KO, Reidpath DD and Kadirvelu A. Review of novel therapeutic targets for improving heart failure treatment based on experimental and clinical studies. Ther Clin Risk Manag 2016; 12: 887-906.

[10] Jha SR, Hannu MK, Chang S, Montgomery E, Harkess M, Wilhelm K, Hayward CS, Jabbour A, Spratt PM, Newton P, Davidson PM and Macdonald PS. The prevalence and prognostic significance of frailty in patients with advanced heart failure referred for heart transplantation. Transplantation 2016; 100: 429-436.

[11] Katz A, Maor E, Leor J and Klempfner R. Addition of beta-blockers to digoxin is associated with improved 1- and 10-year survival of patients hospitalized due to decompensated heart failure. Int J Cardiol 2016; 221: 198-204.

[12] Pitcher D, Soar J, Hogg K, Linker N, Chapman S, Beattie JM, Jones S, George R, McComb J, Glancy J, Patterson G, Turner S, Hampshire S, Lockey A, Baker T, Mitchell S; CIED Working Group. Cardiovascular implanted electronic devices in people towards the end of life, during cardiopulmonary resuscitation and after death: guidance from the resuscitation council (UK), British cardiovascular society and national council for palliative Care. Heart 2016; 102 Suppl 7: A1-A17.

[13] Zafrir B, Salman N, Crespo-Leiro MG, Anker SD, Coats AJ, Ferrari R, Filippatos G, Maggioni AP, Mebazaa A, Piepoli MF, Ruschitzka F, Paniagua-Martin MJ, Segovia J, Laroche C, Amir O; Heart Failure Long-Term Registry Investigators. Body surface area as a prognostic marker in chronic heart failure patients: results from the heart failure registry of the heart failure association of the European society of cardiology. Eur J Heart Fail 2016; 18: 859-868.

[14] Desai AS, McMurray JJ, Packer M, Swedberg K, Rouleau JL, Chen F, Gong J, Rizkala AR, Brahimi A, Claggett B, Finn PV, Hartley LH, Liu J, Lefkowitz M, Shi V, Zile MR and Solomon SD.

Effect of the angiotensin-receptor-neprilysin inhibitor LCZ696 compared with enalapril on mode of death in heart failure patients. Eur Heart J 2015; 36: 1990-1997.

[15] Gori M and Senni M. Sacubitril/valsartan (LCZ696) for the treatment of heart failure. Expert Rev Cardiovasc Ther 2016; 14: 145-153.

[16] Jhund PS, Fu M, Bayram E, Chen CH, Negrusz-Kawecka M, Rosenthal A, Desai AS, Lefkowitz MP, Rizkala AR, Rouleau JL, Shi VC, Solomon SD, Swedberg K, Zile MR, McMurray JJ, Packer M; PARADIGM-HF Investigators and Committees. Efficacy and safety of LCZ696 (sacubitril-valsartan) according to age: insights from PARADIGM-HF. Eur Heart J 2015; 36: 2576-2584.

[17] McMurray JJ, Packer M, Desai AS, Gong J, Lefkowitz MP, Rizkala AR, Rouleau JL, Shi VC, Solomon SD, Swedberg K, Zile MR; PARADIGM-HF Investigators and Committees. Angiotensin-neprilysin inhibition versus enalapril in heart failure. N Engl J Med 2014; 371: 993-1004.

[18] Lu HI, Chung SY, Chen YL, Huang TH, Zhen YY, Liu CF, Chang MW, Chen YL, Sheu JJ, Chua S, Yip HK and Lee FY. Exendin-4 therapy still offered an additional benefit on reducing transverse aortic constriction-induced cardiac hypertrophy-caused myocardial damage in DPP-4 deficient rats. Am J Transl Res 2016; 8: 778-798.

[19] Dutra SGV, Felix ACS, Gastaldi AC, De Paula Facioli T, Vieira S and De Souza HCD. Chronic treatment with angiotensin-converting enzyme inhibitor increases cardiac fibrosis in young rats submitted to early ovarian failure. Auton Neurosci 2017; 206: 28-34.

[20] Yang CC, Yip HK, Chen KH, Sun CK, Chen YT, Chai HT, Sung PH, Chiang HJ, Ko SF, Chung SY, Chen CH, Lin KC, Lin PY and Sheu JJ. Impact of impaired cardiac function on the progression of chronic kidney disease---role of pharmacomodulation of valsartan. Am J Transl Res 2017; 9: 2548-2566.

[21] Yen CH, Leu S, Lin YC, Kao YH, Chang LT, Chua S, Fu M, Wu CJ, Sun CK and Yip HK. Sildenafil limits monocrotaline-induced pulmonary hypertension in rats through suppression of pulmonary vascular remodeling. J Cardiovasc Pharmacol 2010; 55: 574-584.

[22] Lu HI, Lee FY, Wallace CG, Sung PH, Chen KH, Sheu JJ, Chua S, Tong MS, Huang TH, Chen YL, Shao PL and Yip HK. SS31 therapy effectively protects the heart against transverse aortic constriction-induced hypertrophic cardiomyopathy damage. Am J Transl Res 2017; 9: 5220-5237.

[23] Lu HI, Huang TH, Sung PH, Chen YL, Chua S, Chai HY, Chung SY, Liu CF, Sun CK, Chang HW, Zhen YY, Lee FY and Yip HK. Administration of

antioxidant peptide SS-31 attenuates transverse aortic constriction-induced pulmonary arterial hypertension in mice. Acta Pharmacol Sin 2016; 37: 589-603.

[24] Sun CK, Zhen YY, Lu HI, Sung PH, Chang LT, Tsai TH, Sheu JJ, Chen YL, Chua S, Chang HW, Chen YL, Lee FY and Yip HK. Reducing TRPC1 expression through liposome-mediated siRNA delivery markedly attenuates hypoxia-induced pulmonary arterial hypertension in a murine model. Stem Cells Int 2014; 2014: 316214.

[25] Chen YL, Chung SY, Chai HT, Chen CH, Liu CF, Chen YL, Huang TH, Zhen YY, Sung PH, Sun CK, Chua S, Lu HI, Lee FY, Sheu JJ and Yip HK. Early administration of carvedilol protected against doxorubicin-induced cardiomyopathy. J Pharmacol Exp Ther 2015; 355: 516-527.

[26] Day YJ, Chen KH, Chen YL, Huang TH, Sung PH, Lee FY, Chen CH, Chai HT, Yin TC, Chiang HJ, Chung SY, Chang HW and Yip HK. Preactivated and disaggregated shape-changed platelets protected against acute respiratory distress syndrome complicated by sepsis through inflammation suppression. Shock 2016; 46: 575-586.

[27] Lin MJ, Leung GP, Zhang WM, Yang XR, Yip KP, Tse CM and Sham JS. Chronic hypoxia-induced upregulation of store-operated and receptor-operated Ca2+ channels in pulmonary arterial smooth muscle cells: a novel mechanism of hypoxic pulmonary hypertension. Circ Res 2004; 95: 496-505.

[28] Chua S, Lee FY, Chiang HJ, Chen KH, Lu HI, Chen YT, Yang CC, Lin KC, Chen YL, Kao GS, Chen CH, Chang HW and Yip HK. The cardioprotective effect of melatonin and exendin-4 treatment in a rat model of cardiorenal syndrome. J Pineal Res 2016; 61: 438-456.

[29] Chua S, Chang LT, Sun CK, Sheu JJ, Lee FY, Youssef AA, Yang CH, Wu CJ and Yip HK. Time courses of subcellular signal transduction and cellular apoptosis in remote viable myocardium of rat left ventricles following acute myocardial infarction: role of pharmacomodulation. J Cardiovasc Pharmacol Ther 2009; 14: 104-115.

[30] Sun CK, Chang LT, Sheu JJ, Wang CY, Youssef AA, Wu CJ, Chua S and Yip HK. Losartan preserves integrity of cardiac gap junctions and PGC-1 alpha gene expression and prevents cellular apoptosis in remote area of left ventricular myocardium following acute myocardial infarction. Int Heart J 2007; 48: 533-546.

[31] Sun CK, Chang LT, Sheu JJ, Chiang CH, Lee FY, Wu CJ, Chua S, Fu M and Yip HK. Bone marrow-derived mononuclear cell therapy alleviates left ventricular remodeling and improves heart function in rat-dilated cardiomyopathy. Crit Care Med 2009; 37: 1197-1205.

[32] Packer M, McMurray JJ, Desai AS, Gong J, Lefkowitz MP, Rizkala AR, Rouleau JL, Shi VC, Solomon SD, Swedberg K, Zile M, Andersen K, Arango JL, Arnold JM, Bělohlávek J, Böhm M, Boytsov S, Burgess LJ, Cabrera W, Calvo C, Chen CH, Dukat A, Duarte YC, Erglis A, Fu M, Gomez E, Gonzàlez-Medina A, Hagège AA, Huang J, Katova T, Kiatchoosakun S, Kim KS, Kozan Ö, Llamas EB, Martinez F, Merkely B, Mendoza I, Mosterd A, Negrusz-Kawecka M, Peuhkurinen K, Ramires FJ, Refsgaard J, Rosenthal A, Senni M, Sibulo AS Jr, Silva-Cardoso J, Squire IB, Starling RC, Teerlink JR, Vanhaecke J, Vinereanu D, Wong RC; PARADIGM-HF Investigators and Coordinators. Angiotensin receptor neprilysin inhibition compared with enalapril on the risk of clinical progression in surviving patients with heart failure. Circulation 2015; 131: 54-61.